TaN-TiN Binary Alloys and Superlattices as Diffusion Barriers for Copper Interconnects

H. WANG,[1–3] A. GUPTA,[1] ASHUTOSH TIWARI,[1] X. ZHANG,[2] and J. NARAYAN[1]

1.—Department of Materials Science and Engineering, North Carolina State University, Raleigh, NC 27695. 2.—Materials Science and Technology Division, Los Alamos National Laboratory, Los Alamos, NM 87545. 3.—E-mail: wangh@lanl.gov

Binary alloys and superlattices of TaN-TiN thin films were grown on Si(100) substrates with a TiN buffer layer using pulsed laser deposition. A special target assembly was used to manipulate the concentrations of these binary component films. The 60% TaN resulted in a TaN (3 nm)/TiN (2 nm) superlattice, while 30% and 70% TaN generated uniform $Ta_xTi_{1-x}N$ alloys. X-ray diffraction (XRD), transmission electron microscopy (TEM), and scanning transmission electron microscopy (STEM) confirmed the single-crystalline nature of these films. Four-point probe resistivity measurements suggest that these alloy and superlattice films have a lower resistivity than pure single-crystalline TaN films. The Cu-diffusion characteristic studies showed that these materials would have the potential as high-temperature diffusion barriers for Cu in ultra-large-scale integration technology.

Key words: TaN, TiN, superlattice, alloy, Cu diffusion barrier

INTRODUCTION

Titanium nitride (TiN), when considered as a diffusion barrier for Cu interconnects, offers numerous advantages, such as low resistivity, well-controlled microstructure, and well-established process technology in integrated circuit fabrication.[1,2] Compared with TiN, TaN has higher thermal stability, relatively dense interstitial structure, and thickness advantages that fulfill the requirements for next-generation ultra-large-scale integration devices.[3–6] However, TaN has a variety of stable phases (such as solid-solution α-Ta(N), hcp-γ-phase, and hexagonal ε-phase) and metastable phases (such as bcc β-TaN, hexagonal δ-phase TaN, hexagonal WC structure θ-TaN, and B1 NaCl-structured TaN),[7,8] bringing complexities into the fabrication of TaN diffusion barriers.[9–11] Moreover, diffusion barrier materials also act as interconnections between Cu and underlying Si devices. Relatively low resistivity is required for diffusion barriers. Most TaN phases have a much higher resistivity of ~200 μΩ cm than that of single-crystal TiN at ~15 μΩ cm.[2] Recent studies have shown that the metastable cubic TaN (B1 NaCl structure) has a relatively low resistivity compared with other TaN phases, and that it is the only phase that can be integrated with a Si substrate.[12,13] We have recently synthesized a single-crystalline, cubic-TaN phase on Si by using single-crystalline TiN as a buffer layer.[12] The rationale is that TiN can stabilize the metastable cubic-TaN phase because both TiN and cubic TaN have a NaCl structure, and the lattice mismatch between the two materials is less than 2%. Considering the advantages and disadvantages of TaN and TiN, we propose that the binary components of TaN-TiN thin films might be prospective, high-temperature, diffusion-barrier materials with a relatively low resistivity for Cu interconnects.

In this research, we show the successful synthesis of a single-crystalline TaN (3 nm)/TiN (2 nm) superlattice and uniform $Ta_xTi_{1-x}N$ alloys dependent upon the concentration of TaN used in pulsed-laser-deposition experiments. Diffusion studies show that the TaN-TiN superlattice and alloys can be used as a low resistivity, superior diffusion barrier for copper in next-generation integrated circuit devices. In this paper, the microstructure of TaN and TiN

(Received March 31, 2003; accepted May 28, 2003)

superlattices and alloys has been investigated, and a mechanism of superior diffusion-barrier property for these systems has been discussed.

EXPERIMENTAL

The depositions of a TiN buffer layer and TaN-TiN alloys and superlattices were performed in a multi-target chamber with a KrF excimer laser (Lambda Physik [Ft. Lauderdale, FL] 210 $\lambda = 248$ nm, 10 Hz). The targets were hot-pressed, stoichiometric TiN and TaN obtained from CERAC, Inc. (Milwaukee, WI). The target for $Ta_xTi_{1-x}N$ deposition is specially arranged as shown in Fig. 1. The ratio of the area of the two targets can determine the concentration of these as-deposited films and, finally, determine the structure of these films. The TiN buffer layer and various concentration $Ta_xTi_{1-x}N$ samples were deposited at a base pressure of about 1×10^{-8} torr and substrate temperature 650°C ± 10°C. Crystal structure of these films was determined by x-ray diffraction (XRD) using a Rigaku (Rigaku Corp., Tokyo, Japan) x-ray diffractometer with Cu K_α radiation and a Ni filter. Microstructural characterization of these films was performed by cross-section transmission electron microscopy (TEM), high-resolution TEM (HRTEM), and scanning TEM (STEM) using a JEOL–2010F (Japan Electron Optics Ltd., Tokyo) analytical electron microscope with a point-to-point resolution of 0.18 nm (TEM) and 0.12 nm (STEM). Resistivity was measured by the four-point probe technique. For the Cu-diffusion characteristic study, a thin layer of Cu was deposited on each of these alloys at room temperature with back pressure at 1×10^{-8} torr. Post-deposition annealing was then performed at 700°C for 30 min in vacuum at about 1×10^{-6} torr. The diffusion characteristics of Cu into TaN-TiN alloys and superlattice specimens were performed by TEM, HRTEM, and STEM studies.

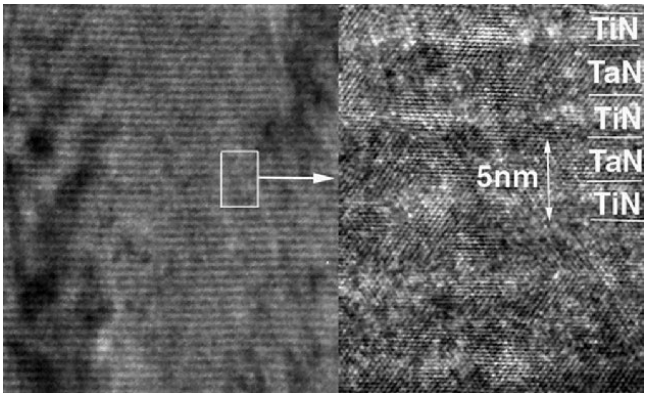

Fig. 1. A schematic diagram of the target assembly of $Ta_xTi_{1-x}N$ alloys and superlattice deposition.

RESULTS AND DISCUSSION

Microstructure of As-Deposited TaN-TiN Alloys and Superlattices

By using the specially arranged target assembly for TaN-TiN deposition, we can determine the ratio of the area of two targets and the concentration of these binary components. To estimate the relative thickness/concentration, we take into account the laser ablation effectiveness. With the concentration at 60% TaN, the TaN-TiN films grew as a TaN/TiN superlattice structure. For x = 30% and x = 70%, the uniform $Ta_xTi_{1-x}N$ alloy was formed. The composition and microstructure of these films are summarized in Table I. The resultant concentrations are measured using a Rutherford backscattering profile and fitted with simulation results.

The XRD patterns (intensity versus 2θ) of the TaN/TiN superlattice ($Ta_{0.6}Ti_{0.4}N$) and the $Ta_{0.7}Ti_{0.3}N$ and $Ta_{0.3}Ti_{0.7}N$ alloys on Si(100) using TiN as a buffer layer are shown in Fig. 2a–c, respectively. In the case of the TaN/TiN superlattice ($Ta_{0.6}Ti_{0.4}N$), the two peaks centered at 42.27° and 93.05° are indexed as $Ta_{0.6}Ti_{0.4}N$ (200) and (400), respectively, suggesting that the superlattice structure has grown highly textured on Si(100). The lattice mismatch between TiN (a = 0.424 nm) and TaN (a = 0.433 nm) is about 1%. The XRD peaks for TaN and TiN layers are overlapped to be a single peak with a lattice parameter of a = 0.4260 nm. Similar peaks were obtained for $Ta_{0.3}Ti_{0.7}N$ and $Ta_{0.7}Ti_{0.3}N$ in XRD patterns. The diffraction peaks of the TiN buffer layer overlapped with that of the $Ta_xTi_{1-x}N$ films. It is interesting to note that the (200) peak shifts slightly with TaN concentration. As the concentration of TaN increases, the (200) peak shifts from 42.31° for $Ta_{0.3}Ti_{0.7}N$ to 42.07° for $Ta_{0.7}Ti_{0.3}N$. Correspondingly, the lattice parameter increased from 0.4280 nm to 0.4310 nm. In the superlattice structure, the B1 cubic-metastable TaN phase has been stabilized by the cubic-TiN buffer layer as well as neighboring thin TiN layers in the superlattice configuration. For the case of uniform alloys, the cubic TaN has been alloyed with TiN and stabilized in the form of a cubic solid solution. To study the in-plane and out-of-plane texture, x-ray phi-scan and rocking curves were performed for all three concentrations, and the resulting angles were within 1.5° and 1°, respectively.

Table I. Comparisons of Various Deposition Concentrations and Resultant Structures for $Ta_xTi_{1-x}N$ Alloys

Target Concentration	Back scattering	Result Structure
$Ta_{0.3}Ti_{0.7}N$	X = 0.33 ± 0.05	$Ta_{0.3}Ti_{0.7}N$ alloy/TiN/Si
$Ta_{0.6}Ti_{0.4}N$	X = 0.58 ± 0.05	TaN (3 nm)/Ti (2 nm) superlattice/TiN/Si
$Ta_{0.7}Ti_{0.3}N$	X = 0.72 ± 0.05	$Ta_{0.7}Ti_{0.3}N$ alloy/TiN/Si

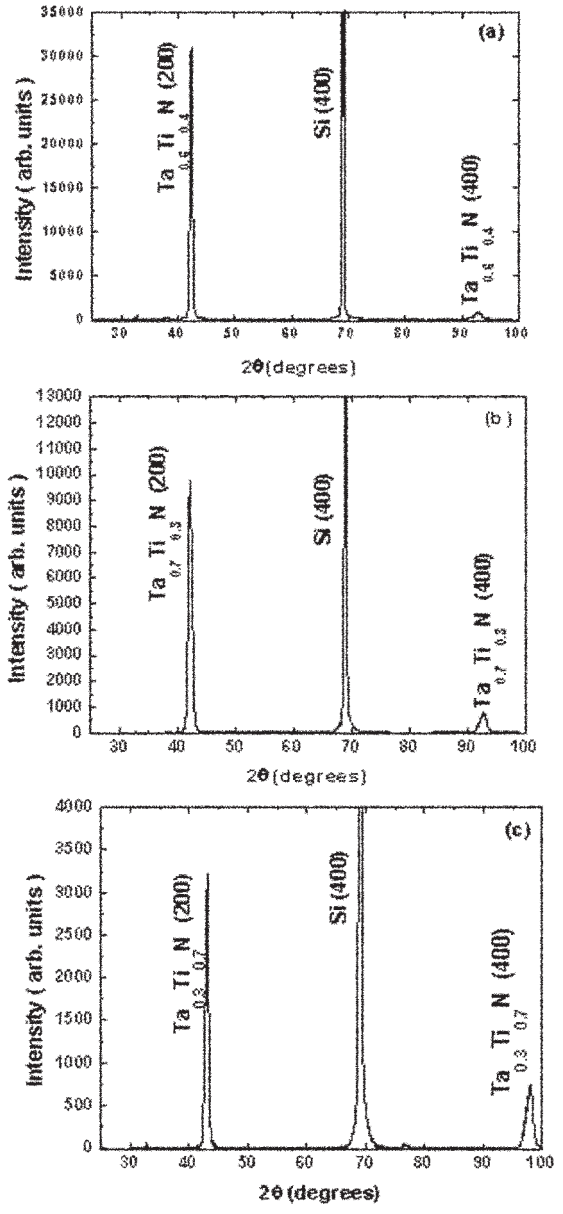

Fig. 2. The XRD patterns for (a) the TaN/TiN superlattice ($Ta_{0.6}Ti_{0.4}N$) and the (b) $Ta_{0.7}Ti_{0.3}N$ and (c) $Ta_{0.3}Ti_{0.7}N$ alloys.

The lattice parameters obtained from XRD studies are very close for the three concentrations. However, their microstructures are quite different as determined from TEM analysis. For the case of $Ta_{0.6}Ti_{0.4}N$, a highly aligned TaN/TiN superlattice formed, whereas uniform alloys formed in the $Ta_{0.3}Ti_{0.7}N$ and $Ta_{0.7}Ti_{0.3}N$ samples. Figure 3 shows the uniform superlattice structure from the <110> cross-section TEM of the TaN/TiN superlattice on Si(100) with a TiN buffer layer. It is clear that the superlattice formed throughout the whole sample above the TiN buffer layer. To study the detailed interface structure between these superlattice layers, HRTEM was performed from the same area, as shown in the inset of Fig. 3. It clearly shows that the superlattice of TaN (3 nm)/TiN (2 nm) has grown epitaxially on top of the

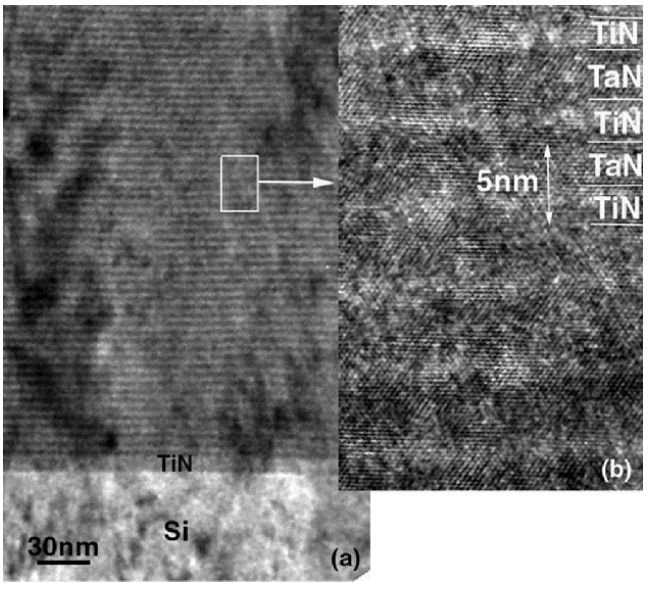

Fig. 3. A low-magnification and high-resolution TEM image of the <110> cross-section sample of the TaN (3 nm)/TiN (2 nm) superlattice ($Ta_{0.6}Ti_{0.4}N$) on Si(100) using a TiN buffer layer.

TiN buffer layer. The interfaces between TiN and TaN are sharp and clean without any indication of interfacial reaction. The {111} lattice planes of these two materials are well aligned. No misfit dislocations are observed along the TaN/TiN interface. This observation could be a result of a small lattice mismatch between TaN and TiN and low interfacial energy, where thickness is less than a critical value. The strain energy is not sufficient to overcome the activation energy for the nucleation of misfit dislocations. Therefore, the dislocation density in this particular superlattice structure is relatively low. Some dislocations are generated from the TiN buffer layer and extend further into the TaN/TiN superlattice. Improving the TiN buffer-layer quality may reduce these types of dislocations.

Selected-area diffraction patterns from the <110> cross-section sample of the TaN/TiN superlattice on Si(100) are shown in Fig. 4. Electron diffractions from the superlattice with substrate and only the superlattice are shown in Fig. 4a and b, respectively. The epitaxial orientation between superlattice, buffer layer, and substrate is analyzed to be superlattice <110> // TiN <110> // Si<110> with a cubic-on-cubic epitaxial relationship. Figure 4b shows only the diffraction from the TaN/TiN superlattice, indicating the growth of a high-quality superlattice with a calculated lattice parameter of 0.4280 nm, very close to TiN. The (200) diffraction spots from the superlattice structure are magnified and are shown in Fig. 4c. Here, the satellite diffraction spots around the diffracted (200) and (400) are clearly seen, indicating that the superlattice structure formed parallel to the (200) plane.

The elemental uniformity of the epitaxial superlattice is studied by STEM in the <110> cross-section

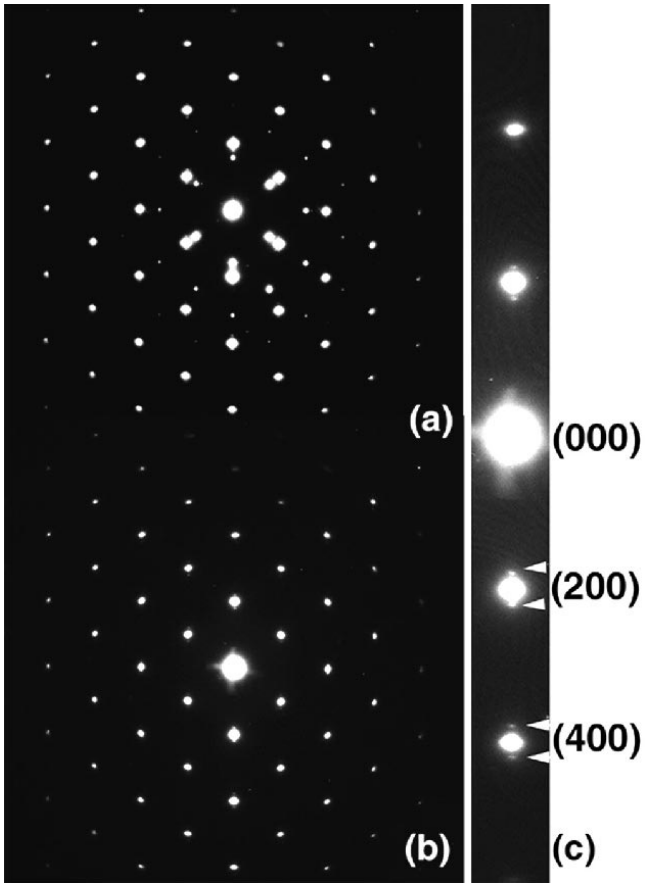

Fig. 4. A selected-area diffraction pattern of <110> cross-section sample of TaN (3 nm)/TiN (2 nm) superlattice ($Ta_{0.6}Ti_{0.4}N$) on Si(100) using a TiN buffer layer: (a) diffraction from films and substrate, (b) diffraction from film only, and (c) magnified (200) diffraction set indicating the satellite feature for superlattice structures.

samples of superlattice TaN/TiN on Si(100). A STEM-Z image from the superlattice, shown in Fig. 5, suggests uniform composition throughout each layer and sharp interfaces between TaN and TiN without interfacial reactions. In Fig. 5, TaN layers appear brighter compared with TiN. This is because the image contrast in STEM-Z is proportional to Z^2, where Z is the atomic number of the element. The atomic number of Ta is 73, much larger than that of Ti, 22.

The $Ta_{0.3}Ti_{0.7}N$ and $Ta_{0.7}Ti_{0.3}N$ formed uniform alloys throughout the thickness, and their microstructures are similar. The cubic epitaxial $Ta_xTi_{1-x}N$ alloys have been stabilized by the TiN buffer layer for both cases. The low-magnification TEM image from the <110> cross-section sample of the $Ta_{0.7}Ti_{0.3}N$ alloy on Si(100) is shown in Fig. 6a. The corresponding selected-area diffraction from the alloy and the Si substrate is shown in Fig. 6b. It is clear that the diffractions spots are clean without satellite structures.

The successful synthesis of single-crystalline, cubic-TaN-TiN alloys and superlattices is a result of using single-crystalline TiN as a buffer layer. The TaN phase directly deposited on Si(100) or Si(111)

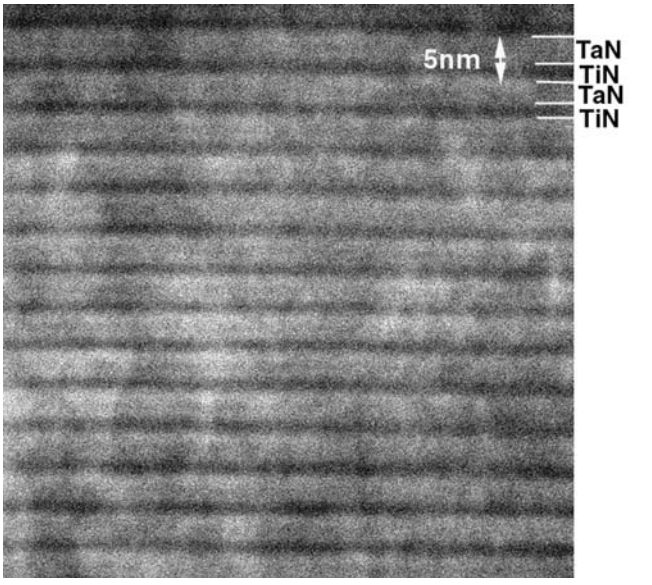

Fig. 5. An STEM (Z-contrast) image from the <110> cross-section sample of the TaN (3 nm)/TiN (2 nm) superlattice ($Ta_{0.6}Ti_{0.4}N$) on Si(100) using a TiN buffer layer, indicating the uniform structure of TaN/TiN superlattice.

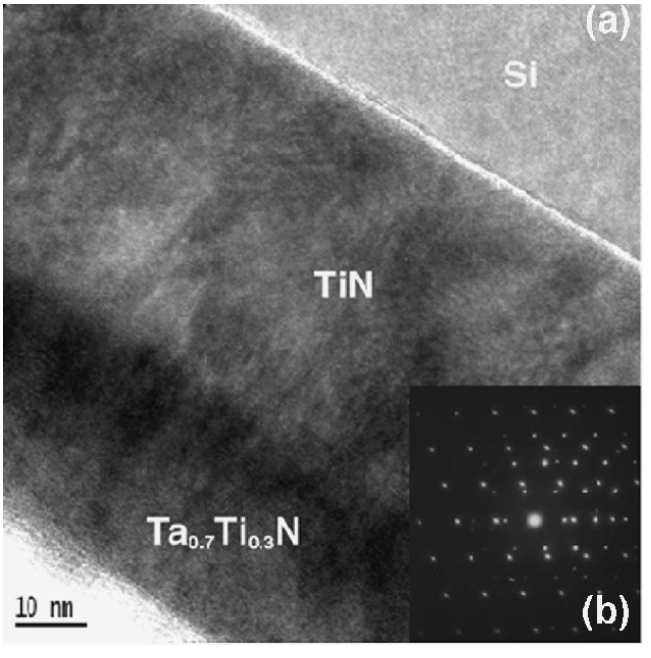

Fig. 6. A low-magnification TEM image and corresponding diffraction pattern of the <110> cross-section sample of the $Ta_{0.7}Ti_{0.3}N$ alloy on Si(100) using a TiN buffer layer, indicating the uniformity and epitaxial growth of alloy structure.

was found to be polycrystalline hexagonal ε-TaN, which is a stable phase of TaN, and is the same phase as the target. The resistivity of this phase is also high. As mentioned before, the lattice mismatch between the metastable, low resistivity, cubic-TaN phase and TiN is less than 2%. The small lattice mismatch between TiN and TaN leads to the epitaxial growth of these two layers. For the case of the

TaN/TiN superlattice, TiN grows on top of the TiN buffer layer via homoepitaxy, while TaN grows on top of TiN via lattice-matching epitaxy. As a result, a highly aligned superlattice was formed with structures very similar to TiN. For the case of the $Ta_xTi_{1-x}N$ alloys, the lattice mismatch between cubic-phase alloys and TiN is even smaller than the mismatch between TaN and TiN. Therefore, the cubic alloys can grow epitaxially on TiN. A single-crystalline, TiN buffer layer can be grown on Si. The interface structure and domain-matching epitaxy of TiN on Si has been discussed in detail elsewhere.[2] Basically, extra half planes are generated in TiN to accommodate the large lattice mismatch (24%). As a result, four columns of TiN atoms grow on top of three columns of Si atoms. This configuration reduces the lattice mismatch between TiN and Si significantly and is, in fact, zero via domain variation DME[2]. This allows the growth of high-quality, single-crystalline TiN on Si.

Electrical Properties of TaN-TiN Alloys and Superlattices

Relatively low resistivity is required for diffusion-barrier materials to ensure the high speed of a circuit, so electrical property is one of the most important properties for diffusion barriers. Electrical resistivity of these $Ta_xTi_{1-x}N$ alloys and the TaN/TiN superlattice over the temperature range of 12–300 K was measured by the four-point probe method. The results are shown in Fig. 7. The TaN/TiN superlattice showed an interesting metallic behavior. The room-temperature resistivity of the TaN/TiN superlattice is around 130 μΩ cm with a rather small, positive temperature coefficient of resistivity (TCR) of 0.002 K^{-1}. For $Ta_xTi_{1-x}N$ alloys, similar electrical characteristics were found. The room temperature resistivity was about 108 μΩ cm for $Ta_{0.3}Ti_{0.7}N$ and 185 μΩ cm for the $Ta_{0.7}Ti_{0.3}N$ alloy. Our measurements show that $Ta_xTi_{1-x}N$ alloys and the TaN/TiN superlattice have relatively lower resistivity than that of TaN.[11,12] Additionally, these systems have positive TCR (metal like) compared to the negative value for TaN. Because of lower values of resistivity and TCR, TaN-TiN alloys and superlattices provide better physical properties as a diffusion barrier compared to TaN.

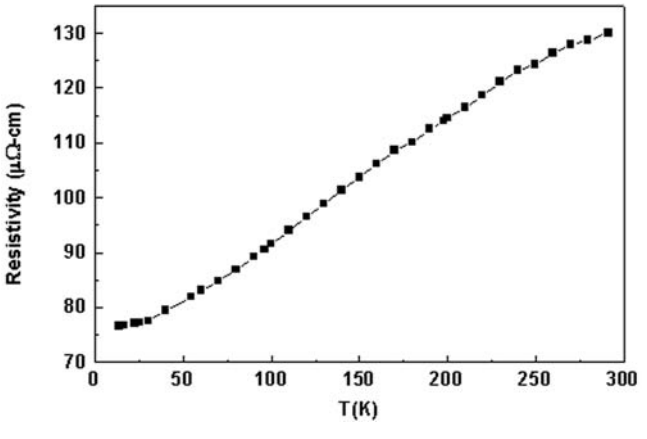

Fig. 7. The resistivity of the epitaxial TaN/TiN superlattice film versus temperature (range from 12 K to 300 K).

Copper Diffusion Characteristics in TaN-TiN Alloys and Superlattices

The Cu-diffusion characteristics in these TaN-TiN alloys and superlattices were studied by TEM, HRTEM, and STEM after annealing at 700°C for 30 min. Figure 8a and b shows the low-magnification and high-magnification TEM images of the <110> cross-section sample of $Cu/Ta_{0.7}Ti_{0.3}N/TiN/Si(100)$ after annealing, respectively. It is obvious that

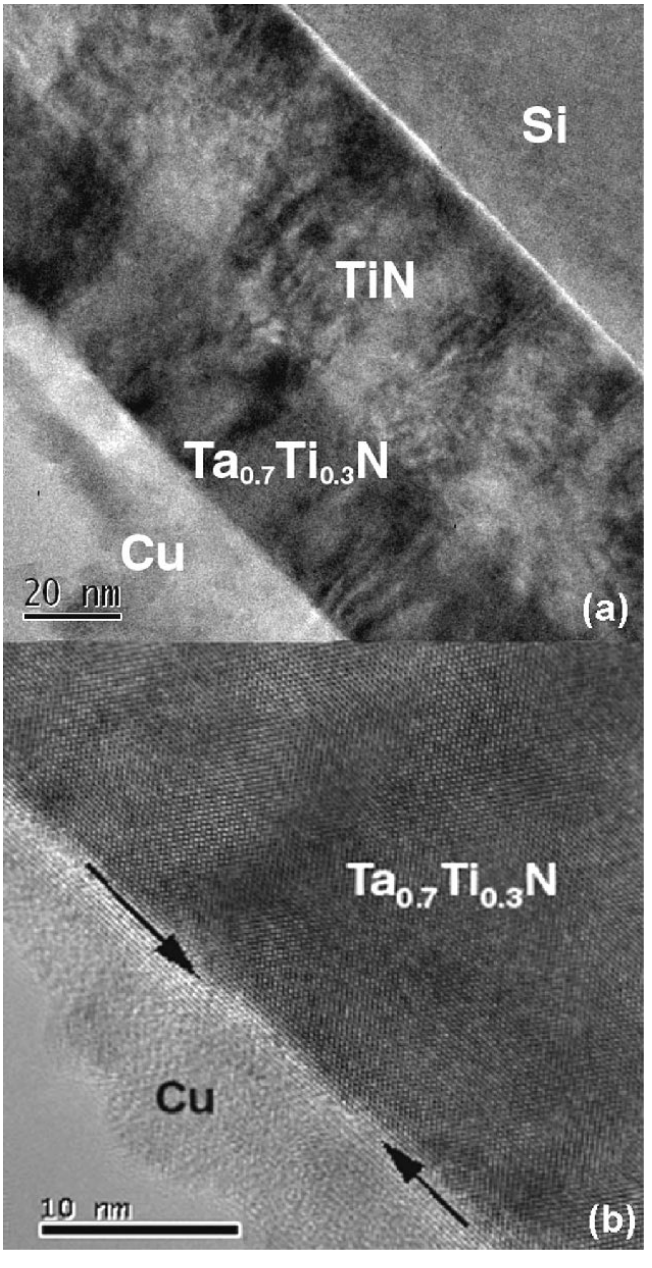

Fig. 8. (a) A low magnification and (b) high magnification of the <110> cross-section sample of the $Cu/Ta_{0.7}Ti_{0.3}N$ superlattice/TiN/Si (100) after 700°C annealing for 30 min.

not only the interface between Cu and $Ta_{0.7}Ti_{0.3}N$ remains very sharp without any indication of diffusion or interfacial reaction, but also the alloy itself remains uniform without any precipitation formed. The HRTEM image even shows epitaxial growth of Cu on $Ta_{0.7}Ti_{0.3}N$ in some areas caused by the annealing at 700°C. Both the $Ta_{0.6}Ti_{0.4}N$ (TaN/TiN superlattice) and $Ta_{0.3}Ti_{0.7}N$ alloy show a similar diffusion-barrier property. The STEM and electron-energy-loss spectroscopy studies of these cross-section samples, though not shown here, further exhibited no indication of any Cu diffusion into these alloys and superlattices, and the interface between Cu and these barriers remains sharp. These studies indicate that both alloy and superlattice systems can be used as a high-efficiency diffusion barrier for Cu interconnects.

CONCLUSIONS

We have investigated the binary alloys and superlattices of TaN-TiN thin films as prospective, diffusion-barrier materials for Cu interconnects. By pulsed laser deposition and a special target configuration, 60% TaN resulted in a superlattice of TaN (3 nm)/TiN (2 nm), while 30% and 70% TaN generated uniform $Ta_xTi_{1-x}N$ alloys. The TiN buffer layers were used to stabilize the cubic, epitaxial binary alloys and superlattices. The single-crystalline nature and uniformity of these superlattice and alloy structures were confirmed by XRD, TEM, HRTEM, and STEM studies. Resistivity measurements and a Cu-diffusion characteristics study indicate that both the TaN/TiN superlattice and $Ta_xTi_{1-x}N$ alloys may serve as a superior diffusion barrier for copper in next-generation integrated circuit devices.

REFERENCES

1. M. Wittmer, B. Studer, and H. Melchiar, *J. Appl. Phys.* 52, 5722 (1981).
2. J. Narayan, P. Tiwari, J. Singh, R. Chowdhury, and T. Zheleva, *Appl. Phys. Lett.* 61, 1290 (1992); J. Narayan, U.S. patent 5, 406,123 (11 April 1995); J. Narayan and B.C. Larson. *J. Appl. Phys.* 93, 278 (2003).
3. M. Stavrev, C. Wenzel, A. Moller, and K. Drescher, *Appl. Surf. Sci.* 91, 257 (1995).
4. S.P. Murarka, *Mater. Sci. Eng. R* 19, 87 (1997).
5. G.S. Chen, S.C. Huang, S.T. Chen, T.J. Yang, P.Y. Lee, J.H. Jou, and T.C. Lin, *Appl. Phys. Lett.* 76, 2895 (2000).
6. M.H. Tsai, S.C. Sun, C.E. Tsai, S.H. Chuang, and H.T. Chiu, *J. Appl. Phys.* 79, 6932 (1996).
7. D. Gerstenberg and C.J. Calbick, *J. Appl. Phys.* 35, 402 (1964).
8. N. Terao, *Jpn. J. Appl. Phys.* 10, 248 (1971).
9. Y.K. Lee, K.M. Latt, K. Jaehyung, T. Osipowicz, C. Sher-Yi, and K. Lee, *Mater. Sci. Eng. B* 77, 282 (2000).
10. K.H. Min, K.C. Chun, and K.B. Kim, *J. Vac. Sci. Technol. B* 14, 3263 (1996).
11. C.-S. Shin, D. Gall, Y.-W. Kim, P. Desjardins, I. Petrov, and J.E. Greene, *J. Appl. Phys.* 90, 2879 (2001).
12. H. Wang, A. Tiwari, A. Kvit, X. Zhang, and J. Narayan, *Appl. Phys. Lett.* 80, 2323 (2002).
13. H. Wang, A. Tiwari, X. Zhang, A. Kvit, and J. Narayan, *Appl. Phys. Lett.* 81, 1453 (2002).